Earthquakes Induced by the Stimulation of an Enhanced Geothermal System below Basel (Switzerland)

Nicholas Deichmann and Domenico Giardini
Swiss Seismological Service, Zürich

INTRODUCTION

To stimulate the reservoir for a "hot dry rock" geothermal project initiated by a private/public consortium in the city of Basel, Switzerland, approximately 11,500 m^3 of water were injected at high pressures between 2 December and 8 December 2006 into a 5-km-deep well below Kleinhüningen (Häring *et al.* 2008). A six-sensor borehole array, installed by the operators of the project at depths between 317 and 2,740 meters around the well to monitor the induced seismicity recorded more than 10,500 seismic events during the injection phase. Hypocentral locations could be calculated for more than 3,000 of these events. The gradual increase in flow rate and wellhead pressure was accompanied by a steady increase in seismicity, both in terms of event rates and magnitudes. In the early morning hours of 8 December, after water had been injected at maximum rates in excess of 50 l/s and at wellhead pressures of up to 29.6 MPa for about 16 hours (Häring *et al.* 2008), a magnitude M_L 2.6 event occurred within the reservoir. This exceeded the safety threshold for continued stimulation, so that injection was stopped prematurely. In the afternoon and evening of the same day, two additional events of magnitude M_L 2.7 and 3.4 occurred within the same source volume. As a consequence, the well was opened and the water allowed to flow back. In the following days about one third of the injected water volume flowed back out of the well (Häring *et al.* 2008). Though the seismic activity declined rapidly thereafter, even more than two years later sporadic microseismicity was being detected in the stimulated rock volume by the downhole-instruments.

The mainshock was felt distinctly in the urban area of Basel. People reported short, high-frequency shaking lasting 1–3 seconds, often accompanied by a loud bang similar to an explosion. The bang contributed significantly to the frightening effect that this experience had on many witnesses. Typical macroseismic effects were creaking of woodwork and rattling of doors and windows. From the city as well as from neighboring communities, very small nonstructural damage was consistently reported for hundreds of buildings, such as hairline cracks to the plaster or damage to the paint at building junctions. Although often difficult to verify, a significant share of the reported instances of damage is presumed to be a direct consequence of the earthquake. Thus macroseismic intensity in the different parts of Basel and the neighboring municipalities ranges from IV to V according the EMS98 scale. As a consequence of how the largest of these induced earthquakes was perceived by the public and the damage that it allegedly caused, the project was put on hold, pending a comprehensive assessment of the seismic risk associated with its continuation.

Meanwhile, despite the temporary setback with respect to the original plan, efforts to analyze the large amount of data generated by this project have produced preliminary results, some in the form of internal reports to the sponsor (Geopower Basel AG) and others as publications in the open literature. An overview of the project, including a documentation of injection pressures and flow rates, can be found in Häring *et al.* (2008). First analyses of the induced microseismicity have been published by Kumano *et al.* (2007), Asanuma *et al.* (2007), and Dyer *et al.* (2008). Under contract from Geopower Basel AG, the Swiss Seismological Service (SED) performed an extensive study that includes seismotectonic aspects, scaling relationships between local magnitude (M_L) and moment magnitude (M_w), statistical analyses of the temporal and spatial evolution of the microseismicity, and ground-shaking scenarios for possible stronger events based on macroseismic models and numerical calculations (SED 2007). The main results of this study have been summarized by Kraft *et al.* (2009). A presentation of the numerical and macroseismic earthquake scenarios as well as detailed documentation of the focal mechanisms available to date have been submitted for publication (Ripperger *et al.* forthcoming; Deichmann and Ernst forthcoming).

The present article is based on the analysis of the 195 strongest events recorded by SED between 2 December 2006 and 30 November 2007. The main goal is to document the spatial and temporal evolution of the induced seismicity and to discuss the available focal mechanisms in light of the recent spontaneously occurring earthquakes in the Basel region and stress observations in the borehole as documented by Valley and Evans (2006, forthcoming).

doi: 10.1785/gssrl.80.5.784

TECTONIC SETTING

Basel is located at the southern end of the Rhine Graben, where it intersects the fold and thrust belt of the Jura Mountains of Switzerland (Figure 1, Table 1). As such it is an area that in the geologic past has seen both extension (rifting phase of the Rhine Graben) and thrusting (folding of the Jura Mountains). A recent comprehensive summary and an exhaustive reference list of the evolution of the Upper Rhine Graben and Jura Mountains throughout geologic time can be found in Ustaszewski and Schmid (2007).

As a consequence of its tectonic evolution, the Upper Rhine Graben constitutes a zone of weakness in the mid-European lithosphere, where strain is localized and tectonic stress is released. This is documented by significant seismic activity all along the Rhine Graben, in particular at its southern end. In fact, in 1356, Basel was the site of the strongest historically known earthquake in Europe north of the Alps, and minor earthquakes have been known to occur ever since. Focal mechanisms of recent earthquakes show a predominance of strike-slip and normal faulting on either NNE-SSW (Rhenish) or WNW-ESE (Hercynic) striking faults (Figure 1). These focal mechanisms are thus compatible with an overall NW-SE oriented shortening of the lithosphere expected from the large-scale interaction between the opening of the Atlantic and the collision between the African and the European continental plates.

The borehole itself is situated at the southern end of the Rhine Graben. As shown in the lithological section reproduced in Valley and Evans (forthcoming), it penetrates a 2,426-m-thick sedimentary sequence before entering the crystalline basement. The borehole casing reaches a depth of 4,629 m, and the open-hole section extends down to a depth of 5,000 m (Häring *et al.* 2008).

SEISMIC NETWORKS

The seismic data analyzed in this article were recorded by several different seismometer and accelerometer networks operated by three separate institutions: Schweizerischer Erdbebendienst (SED), Landeserdbebendienst Baden-Württemberg (LED), and Geothermal Explorers Ltd. (GEL). The corresponding stations are listed in Table 2 and the locations of the stations are shown in Figures 1 and 2. This compilation does not include all potentially available seismic stations; only those from which data were actually used in the analysis of the seismicity associated with the Basel geothermal project are included.

The borehole sensors are short-period geophones with a natural frequency between 4.5 and 5 Hz and a damping coefficient of 0.21. The data was recorded at an original sampling rate of 1000 Hz, but the signals transmitted to the SED were decimated to 500 Hz (OTER1 120 Hz). In the shallower boreholes, all three orthogonal components are inclined at an angle of 54.7 degrees, but their horizontal orientation is not known. In the deepest monitoring well (OTER2) the three components are mounted in the traditional way with one vertical and two horizontals, but again the horizontal orientation is

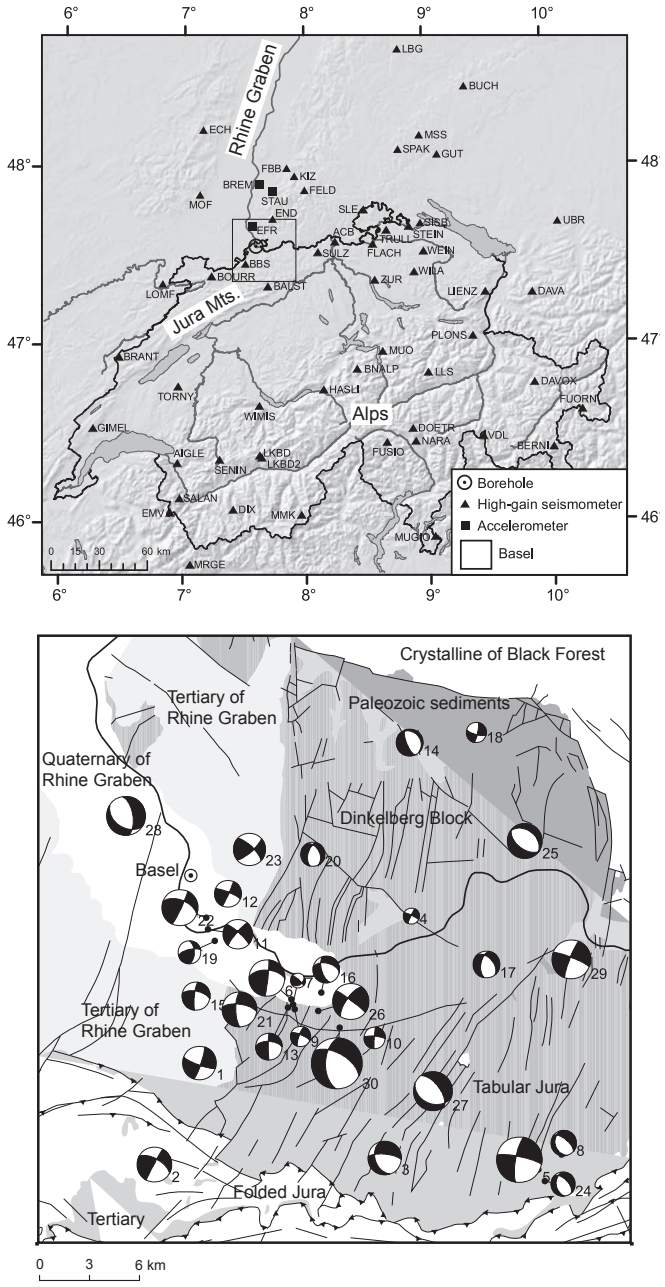

▲ **Figure 1.** Top: Topographic map of Switzerland and surroundings with regional seismic stations that contributed data to this study. Bottom: Tectonic map of the Basel area with focal mechanisms of tectonic earthquakes since 1982. The number next to each mechanism corresponds to the event number in Table 1. The location of the Basel geothermal borehole is indicated by the circle with the black dot. The tectonic background is from the Digital Tectonic Map of Switzerland.

not known. The high-gain network of the SED consists mainly of STS-2 broad-band seismometers and to a lesser degree of 1- and 5-second seismometers. Their signals are digitized at a sampling rate of 120 Hz. The high-gain network of the LED consists 5 of 1-second seismometers and their signals are digitized at sampling rates between 62.5 and 125 Hz. Most of the accelerometer data of the SED is available at sampling rates of

TABLE 1

Focal mechanism parameters of the natural seismicity in the Basel region. Evn: event number in Figure 1; Time: UTC; Z: focal depth (km); M: local magnitude (M_L) calculated by SED; Nodal Planes: strike/dip/rake; P- and T- Axes: azimuth/plunge; F: focal mechanism type (after Zoback, 1992)— SS strike-slip, NF normal fault, NS normal strike-slip, UD undetermined. References: 5 Deichmann (1987), 13 Deichmann & Garcia-Fernandez (1992), 18 Bonjer (1997), 28 Deichmann *et al.* (2000), 29 Baer *et al.* (2001), 31 Deichmann *et al.* (2002), 35 Deichmann *et al.* (2004), 37 Baer *et al.* (2005).

vn	Date	Time	Lat	Lon	Z	M	Plane 1	Plane 2	P	T	F	Location (Ref.)
1	1982/03/25	18:45	47.487	7.601	7	2.5	110/79/-172	018/82/-011	334/13	064/02	SS	Reinach (18)
2	1984/04/10	16:50	47.432	7.565	22	2.6	300/62/-176	208/87/-028	160/22	257/17	SS	Breitenbach (5)
3	1984/04/12	00:50	47.435	7.748	21	2.5	162/42/-030	275/71/-128	143/49	032/17	NS	Bubendorf (5)
4	1986/11/01	04:01	47.565	7.77	19	1.2	296/81/-174	205/84/-009	160/11	251/02	SS	Dinkelberg (18)
5	1987/04/11	03:14	47.428	7.87	7	3.4	190/76/-011	282/79/-166	146/18	056/02	SS	Läufelfingen (13)
6	1987/12/16	09:36	47.521	7.675	9	2.7	006/86/ 036	273/54/ 175	134/21	236/28	UD	Pratteln (28)
7	1987/12/31	15:16	47.518	7.676	12	1.1	053/40/ 014	312/81/ 129	013/26	258/41	UD	Pratteln (18)
8	1988/04/16	14:05	47.436	7.889	9	1.9	310/63/-108	165/32/-059	187/67	053/16	NF	Zeglingen (13)
9	1988/05/11	11:12	47.515	7.677	10	1.5	199/75/-016	293/75/-164	156/22	066/00	SS	Pratteln (18)
10	1988/10/27	20:52	47.5	7.741	12	1.6	275/77/-177	184/87/-013	139/11	230/07	SS	Liestal (28)
11	1989/05/05	17:44	47.559	7.609	10	2.2	312/79/-170	220/80/-011	176/15	266/01	SS	Basel (18)
12	1990/06/16	22:41	47.576	7.619	18	2	293/80/ 177	024/87/ 010	158/05	249/09	SS	Weil (18)
13	1990/07/25	14:38	47.516	7.672	10	2	180/86/-032	272/58/-176	131/25	231/19	SS	Pratteln (18)
14	1990/07/31	19:13	47.659	7.77	19	2	318/21/-109	158/70/-083	080/64	243/25	NF	Steinen (18)
15	1990/08/16	18:39	47.523	7.599	11	2.1	282/61/-167	186/79/-030	140/29	237/12	SS	Reinach (28)
16	1990/11/08	19:38	47.524	7.698	11	2	282/50/-141	164/61/-047	127/53	225/06	NF	Pratteln (28)
17	1990/11/28	01:38	47.539	7.83	18	2	319/48/-130	190/55/-055	159/61	256/04	NF	Möhlin (18)
18	1991/05/20	00:13	47.664	7.823	17	1.5	105/73/-170	012/80/-017	328/19	059/05	SS	Hausern (18)
19	1991/06/04	17:17	47.552	7.614	7	1.7	360/56/ 024	256/70/ 144	311/09	213/39	SS	Basel (18)
20	1991/11/05	09:13	47.599	7.692	17	1.8	334/43/-122	194/55/-064	160/68	266/07	NF	Lörrach (18)
21	1992/03/25	05:33	47.515	7.633	8	2.6	278/65/-160	179/72/-026	137/31	230/05	SS	Muttenz (28)
22	1996/04/24	09:36	47.565	7.607	12	2.7	292/55/ 174	025/85/ 035	153/20	254/28	SS	Basel (28)
23	1996/06/15	01:05	47.602	7.642	21	2.4	314/73/ 165	048/76/ 017	180/02	271/23	SS	Basel (28)
24	1997/02/21	05:04	47.422	7.875	8	1.8	316/55/-114	174/42/-060	171/69	063/07	NF	Läufelfingen (28)
25	1997/09/02	00:30	47.606	7.861	23	2.6	128/53/-090	308/37/-090	038/82	218/08	NF	Möhlin (28)
26	1999/07/13	20:47	47.514	7.696	19	2.7	215/70/-005	307/85/-160	173/17	079/11	SS	Pratteln (28)
27	2000/06/20	06:19	47.471	7.787	18	2.9	111/35/-118	324/60/-072	273/70	041/13	NF	Sissach (29)
28	2001/04/12	07:07	47.62	7.543	8	2.9	123/40/-130	351/61/-062	308/63	061/11	NF	Bâle-S.Louis (31)
29	2003/08/31	05:39	47.542	7.898	17	2.9	292/82/-172	201/82/-008	156/11	246/00	SS	Zeiningen (35)
30	2004/06/21	23:10	47.505	7.713	22	3.8	182/53/-041	300/58/-135	154/53	060/03	NF	Liestal (37)

250 Hz, with some of the older off-line stations recording at sampling rates varying between 128 and 256 Hz, whereas the LED accelerometer signals are sampled at 100 Hz.

The data from the borehole sensors of GEL and of the high-gain permanent seismometer network, as well as of the online accelerometers of SED, were available in real- or near real time and thus provided the basis for continuous monitoring of the ongoing seismicity. The records from all other networks had to be downloaded or requested manually and then partly reformatted and integrated into the existing data files. They were thus not available for a first routine location but only for a subsequent, more detailed analysis, in particular for the calculation of focal mechanisms.

ROUTINE DATA ANALYSIS

Event Detection

The data monitored continuously and in real time at SED were the signals from the permanent high-gain network, the online accelerometers, and the borehole sensor at station OTER1. Event detection and preliminary automatic hypocenter location and magnitude determination were based on the high-gain network and on OTER1. Once an event was detected, the additional data from the other borehole sensors and from the accelerometers available online were automatically integrated into the waveform files (within a few minutes after the event) and were then available for a manual evaluation by a seismologist. An event was detected whenever the threshold criteria

TABLE 2

List of stations and instruments of the networks that supplied data for the present study. The networks were operated by Geothermal Explorers (GEL), the Swiss Seismological Service (SED) and the Landeserdbebendienst Baden-Württemberg (LED). The corresponding station maps are reproduced in Figures 1 and 2 of the article.

GEL borehole sensors (in parenthesis is the depth below surface in m):
OTER2 (2740), OTER1 (500), JOHAN (317), HALTI (542), MATTE (553), RIEH2 (1213)

SED high-gain seismometer-network:
BALST, BOURR, SULZ, ACB, SLE, FLACH, ZUR, TRULL, STEIN, WILA, BNALP, HASLI, WIMIS, TORNY, MUO, WEIN, BRANT, LKBD, LKBD2, LLS, SENIN, AIGLE, LIENZ, PLONS, FUSIO, GIMEL, DOETR, NARA, SALAN, DIX, MMK, EMV, VDL, DAVOX, MUGIO, FUORN, BERNI, SENIN, DAVA, MRGE

SED online accelerometers:
BOTTER, SBAF, SRHB, SBAP, SBAT SBIS SMZW SKAF SAUR

SED offline accelerometers:
SBAE SBAJ SBAM SBEG SBIF SMZA SCHC SRNR

SED offline temporary accelerometers:
CHBAL, CHBBO, CHBRI, CHBMU, CHBDO, CHBPF

LED high-gain seismometer-network:
BBS, FELD, MOF, FBB, LOMF, ECH, SISB, SPAK, GUT, KIZ, LBG, BUCH, UBR, END, MSS

LED high-gain temporary seismometers:
WL8, WL11, WL12

LED accelerometers:
BREM, EFR, STAU, WEIL, WYH, LOER, LOES, WL2, WL7, WL9, WL10

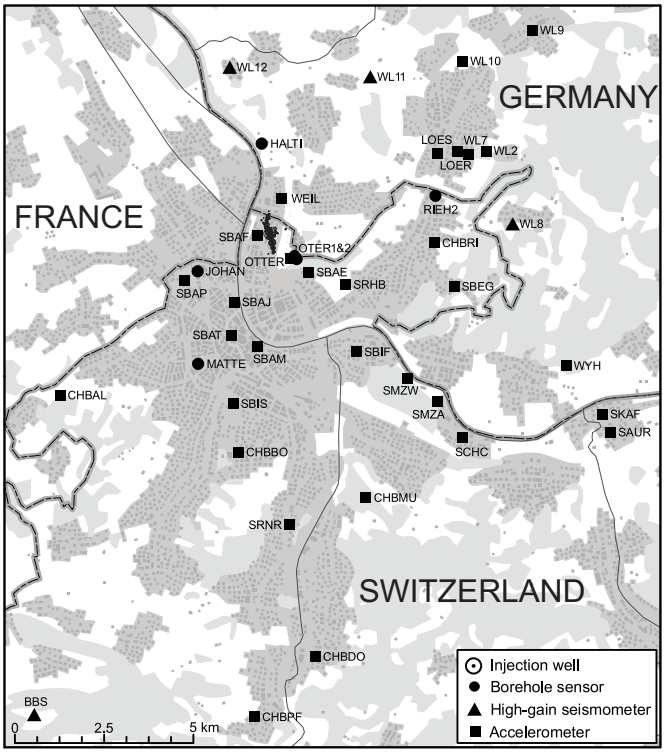

▲ **Figure 2.** Seismic stations in Basel and surroundings during the stimulation in December 2006 and for about six months thereafter. The darker shaded areas correspond to the city of Basel and surrounding towns, while woodland and farmland are the light gray and white patches. The epicenters of the induced seismicity and the Basel injection well are located immediately east of station SBAF and in between stations WEIL and OTTER.

were met by at least four stations. In the case of events in the Basel area, the significant stations are the borehole sensor at OTER1 and the three closest stations of the SED high-gain network, BALST, BOURR, and SULZ, located at epicentral distances of about 30–40 km (Figures 1 and 2). Therefore, the detection sensitivity of the SED for events in the Basel area is considerably lower than that of GEL, which is based on the signals recorded by the six borehole stations in the immediate vicinity. Between 3 December 2006 and the end of November 2007, the SED detected and located 195 events in the immediate vicinity of the borehole site in Basel with local magnitudes (M_L) ranging between 0.7 and 3.4. Thus the resulting sensitivity was amply sufficient for detecting those events about which it was deemed necessary to inform the public in near real time. However, since July 2007, the detection sensitivity of the SED has decreased somewhat due to the removal of the sensor at OTER1.

Hypocenter Locations

In general, routine manual data analysis of the Basel events consisted of picking arrival times at all borehole stations, at the online strong-motion stations (accelerometers) in and around Basel, and at all SED high-gain stations for which the signal-to-noise ratio was sufficiently high. The routine analysis of the first induced events, which were assumed to occur in the immediate vicinity of the open section of the injection borehole, showed that the most consistent hypocenter locations are obtained by using the *P*- and *S*-arrival times of the borehole stations together with the *P*-arrival times of the accelerometers within a region

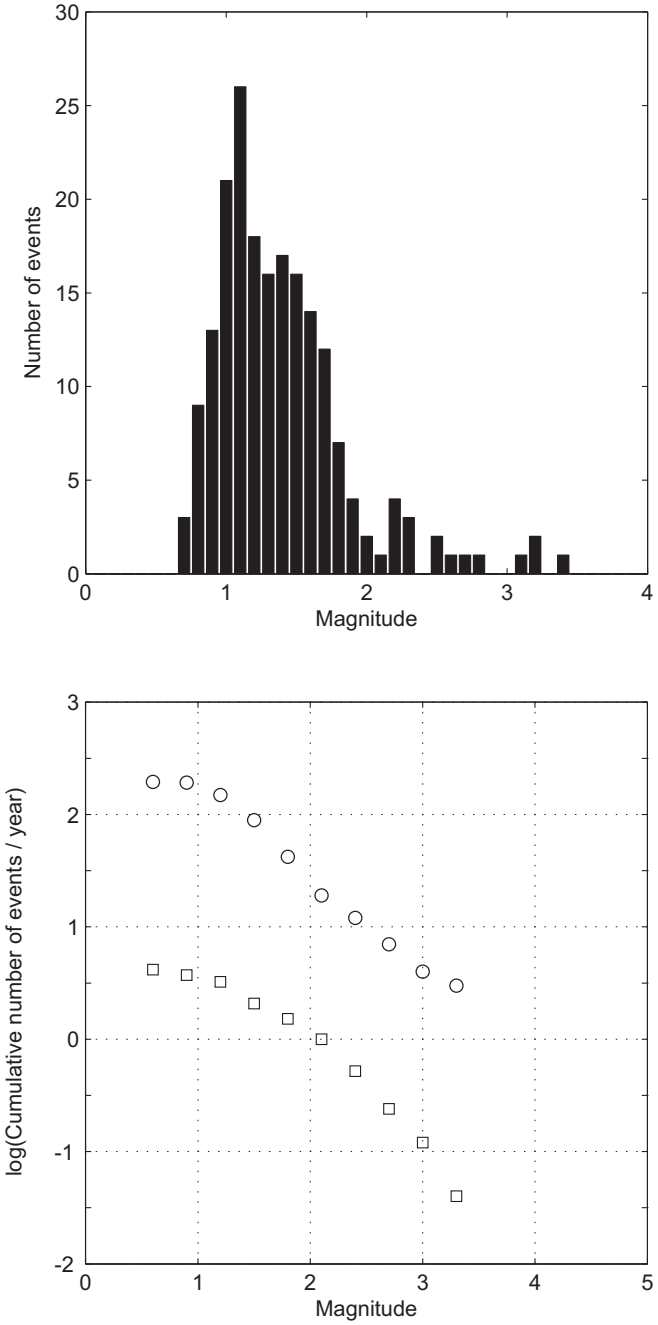

▲ **Figure 3.** Top: Magnitude histogram of the induced seismicity in Basel recorded by the Swiss Seismological Service (2006/12/03–2007/11/30). Bottom: Cumulative number of events per year as a function of local magnitude (M_L), in bins of 0.3 magnitude units, of the induced seismicity (circles) and of the natural seismicity (squares) in the region outlined in Figure 2, averaged over the years 1984–2008.

of about 12 km around the borehole. Arrivals at stations of the Swiss and German regional networks situated at larger epicentral distances were not used for locating the events. The locations were calculated with a probabilistic nonlinear gridsearch algorithm, using a three-dimensional velocity model derived for Switzerland and the surrounding area from the results of local earthquake tomography and controlled source seismology (Husen *et al.* 2003). The epicenters form a cluster with a maximum dimension of about 1.5 km. Computed focal depths are between 4 and 5 km. The locations listed on the Web site of the Swiss Seismological Service (http://www.seismo.ethz.ch/basel) are given with a precision of 0.001 degrees for the epicenters (equivalent to about 0.11 km in NS and 0.075 km in EW direction) and 1 km for the focal depth. The absolute location error of a single event estimated from the result of the location algorithm is about 1 km for the epicenter coordinates and 1.2 km for the focal depth. However, from a comparison with the results of the more precise master event location method presented later in this paper, the relative locations of the epicenters within the cloud are in general more precise than 1 km.

Magnitude Determination

One of the main purposes for SED involvement in the continuous monitoring of the induced seismicity was to determine and communicate to the public a magnitude value for potentially felt events that is immediately comparable to routinely determined local magnitudes (M_L) of natural earthquakes in Switzerland. Since the distance attenuation relations are not calibrated for distances smaller than about 10 km, let alone for high-frequency borehole seismometers, M_L was calculated following standard SED procedures. A separate magnitude value is calculated from the maximum amplitude of the Wood-Anderson–filtered horizontal component seismograms recorded at each station of the permanent high-gain network of the SED. The resulting magnitude value for a given earthquake corresponds to the median of the individual station magnitudes. A histogram of the local magnitudes of all events recorded by SED is shown in Figure 3. The magnitude of completeness for this dataset is estimated to be around (M_L) 1.1 or 1.2. As can be seen from the frequency-magnitude diagram in Figure 3, the 195 events induced by the geothermal reservoir stimulation over the period of 12 months constitute a very significant increase in the level of seismic activity compared to the four events per year in the same magnitude range averaged over the time between 1984 and 2008 that occurred naturally in the area outlined in Figure 2.

The stations that supplied most of the magnitude data are BALST, BOURR, SULZ, and SLE (Figure 1). An analysis of the scatter of the individual station magnitudes shows that on average, the values of these four stations deviate systematically by +0.2, -0.2, -0.1, and +0.5 from the resulting median magnitude value. The large deviation (+0.5) of the magnitude observed at station SLE is probably due to the fact that this station is located at a distance from Basel (70 km) at which the maximum amplitude happens to coincide with a particularly energetic *S*-wave reflection from the Moho (*SmS*). The observed scatter of the individual station magnitudes suggests that the uncertainty of most of the resulting M_L determinations is likely to be on the order of ±0.2. For each event for which more than four magnitude values are available, we examined the difference between the resulting M_L value and the median value of the four stations BALST, BOURR, SULZ, and SLE. The mean

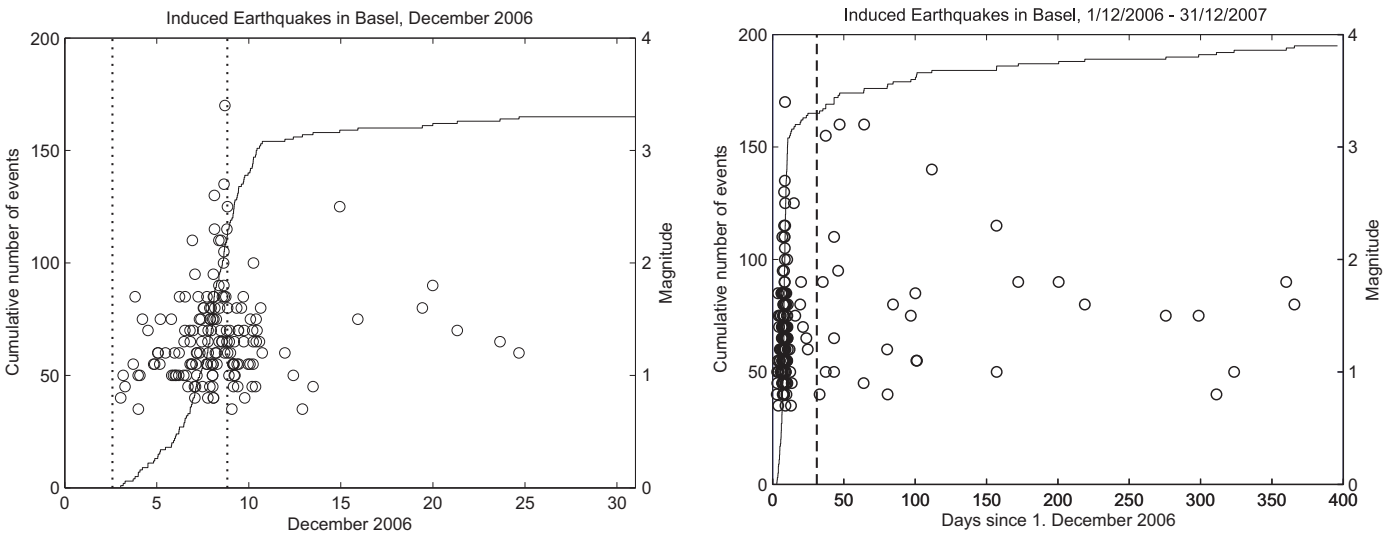

▲ **Figure 4.** Cumulative number of events (stepwise continuous curves) and local magnitudes, M_L, (circles) of the induced seismicity in Basel recorded by the Swiss Seismological Service from 1 December 2006 until 31 December 2007. The left panel shows an enlargement of the first month included in the right panel, and the dashed vertical line on the right marks December 31, 2006. The two dotted vertical lines in the left panel mark the beginning and end (bleed-off) of stimulation. Note the abrupt change in slope of the curve of the cumulative number of events (and thus in seismic activity) on 11 December 2006.

of this difference is -0.093 and the median is 0.1. This means that on average for these events we would be overestimating the magnitude by about 0.1, if we relied only on these four stations. This also implies that the magnitude values of many of the small events (magnitudes less than about 1.7) might be overestimated by about 0.1 relative to the larger events.

Temporal Evolution of the Seismic Activity

Although the events recorded by the SED represent only a small fraction of the total seismicity induced by the geothermal reservoir stimulation in Basel, it is instructive and useful for subsequent analyses of the data to examine the temporal evolution of the occurrence of these events. The activity can be subdivided into four phases (Figure 4): a first phase during stimulation that reached its peak, both in terms of number of events and in terms of maximum magnitudes, on December 8, followed by a phase of declining activity through to the end of the year, then a renewed increase of activity starting at the beginning of 2007, and finally a period of persistent but gradually decreasing unrest since mid-February 2007. Note that the third phase at the beginning of 2007, one to two months after the end of stimulation, includes three $M_L > 3$ events. As of the beginning of June 2009, the last event that was detected by the SED occurred on 30 September 2007, with M_L 1.6. However, the borehole network operated by GEL continues to record smaller events, some of which are strong enough to be locatable.

MASTER-EVENT RELOCATION

Method

In general, hypocenter locations are subject to two main sources of error—errors in picking the onset times of the seismograms and errors in the seismic velocity model. Often the absolute location of a set of epicenters is less important than the location of the events relative to each other. In these cases it is useful to relocate the events with one of several relative location procedures, such as joint hypocenter determinations, double-difference algorithms, or master-event methods. Common to all these methods is the assumption that the set of hypocenters to be located relative to each other occupies a restricted volume in space, for which errors in the velocity model are identical and therefore do not affect the relative locations. In the case of the induced seismicity in Basel, an additional seismometer was installed near the casing shoe in the injection borehole (BS1) during the initial stimulation phase. Thus the absolute locations of the first few events, which occurred in the vicinity of the borehole, can be determined with high precision. We have therefore chosen to apply a master-event relocation procedure to the 195 events recorded by SED, using the M_L 1.7 earthquake of 3 December 2006, 19:51, as the master event.

In this procedure we fixed the location of the master event to the absolute location calculated by GEL using the temporary seismometer in BS1 and determined the *P*- and *S*-wave travel times to the six borehole sensors. All other events are then relocated relative to the master event by using the travel-time residuals of this event as station corrections.

As a consequence, the relative locations calculated in this manner are only a function of the travel-time differences between master- and slave-events and of the seismic velocities in the source region. Given that all hypocenters are located in the crystalline basement, we assumed a *Vp* value of 5.95 km/s and a *Vp/Vs* ratio of 1.72, which are close to the values used by GEL for its absolute locations. The remaining relative location errors are then merely a function of inconsistent arrival-time picks from one event to the other and to a lesser degree of the velocity errors in the hypocentral region. As with most

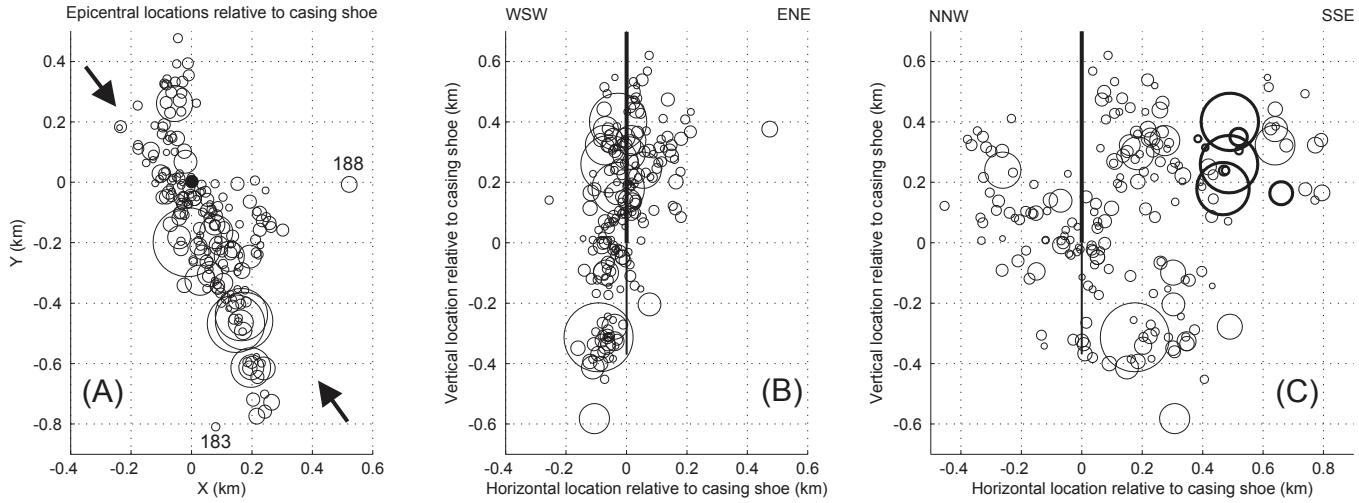

▲ **Figure 5.** Epicenter plot (A) and depth cross-section of the master-event locations, perpendicular (B) and parallel (C) to the general trend of the epicenter alignment, relative to the casing shoe (beginning of the open-hole section). In (A) the well is marked by the black dot (0,0); in (B) and (C) the cased section of the well is marked by the thick line and the open hole section by the thin line. The size of each circle is proportional to the seismic moment of the event. The largest circle at a depth between -0.2 and -0.3 km represents the M_L 3.4 mainshock of 8 December 2006. The nine circles in the depth interval between +0.1 and +0.5 km plotted with heavier lines in panel (C) correspond to the events that occurred between 1 January and 2 February 2007 and include the three $M_L > 3$ post-stimulation events. Event nos. 183 and 188 label the two outlier events discussed in the text. The arrows in panel (A) point in the direction of maximum horizontal compressive stress derived from wellbore failure measurements in the crystalline basement down to 5 km depth by Valley and Evans (2006, forthcoming).

other location algorithms, the relative locations are calculated by a least-squares adjustment of the relative travel-time residuals. The latter are more than one order of magnitude smaller than the absolute travel-time residuals. Thus, effectively, the improvement in the consistency of the relative locations is mainly due to the fact that the scatter in the locations, caused by having to use different combinations of stations and phase readings for different events, is reduced by virtue of adjusting these much smaller residuals.

In the adopted least-squares algorithm, the individual phase readings are weighted by the inverse of an assumed timing uncertainty for each pick, and the resulting location error is calculated from the square root of the diagonal elements of the inverse of the so-called normal-equations. Consequently the calculated location errors are a function of the number of phase readings as well as of the hypocenter location relative to the station configuration and are directly proportional to the assumed timing uncertainties. These location errors are given for the *x, y,* and *z* coordinates. If the station geometry is strongly asymmetric relative to the hypocenter location, these coordinate directions can deviate from the orientation of the axes of the error ellipsoid, and as a consequence the true errors will be underestimated. For the combination of station configuration and hypocenter locations encountered in the case of the induced seismicity in Basel, Monte Carlo simulations with the assumed arrival-time uncertainties demonstrate that the calculated errors correspond to one standard deviation of the true location scatter.

Results of the Master-event Relocation

The results of the master-event relative locations for the 195 events recorded by SED between 2 December 2006 and 30 November 2007 are shown in Figure 5. The absolute location of the master event determined by GEL places it 9 m to the east and 53 m to the south of the well and 48 m below the casing shoe. These values have been used to plot the hypocenters of all other events relative to the casing shoe. For the first 185 events, we used only arrivals recorded by the borehole sensors. For event 187 (2007/05/21 04:19) the number of available borehole arrivals is not sufficient for a stable solution. Therefore, for this and all following events we included arrivals recorded by the online strong-motion stations within an epicentral distance of about 12 km. Tests on some of the earlier well-recorded events showed that using data from the strong-motion stations changes the relative locations by significantly less than the computed standard errors. Based on a visual assessment of the manual timing accuracy of the various arrivals, the assumed timing errors used for the relative locations are 0.01 s for the *P* waves and 0.01–0.025 s for the *S* waves at the borehole sensors. Taking into account the lower sampling rate and frequency content of the signals, the assumed uncertainties for the *P* and *S* arrivals at the strong-motion stations are 0.02 and 0.04 s. The mean and standard deviations of the calculated relative location errors for the *x*, *y*, and *z* coordinates are 49 ± 4 m, 54 ± 6 m, and 72 ± 8 m. Although it is theoretically not justifiable to use the observed travel-time residuals as a measure for the observation uncertainty of individual arrival-time picks, the fact that the average of the root mean squares (rms) of these residuals over

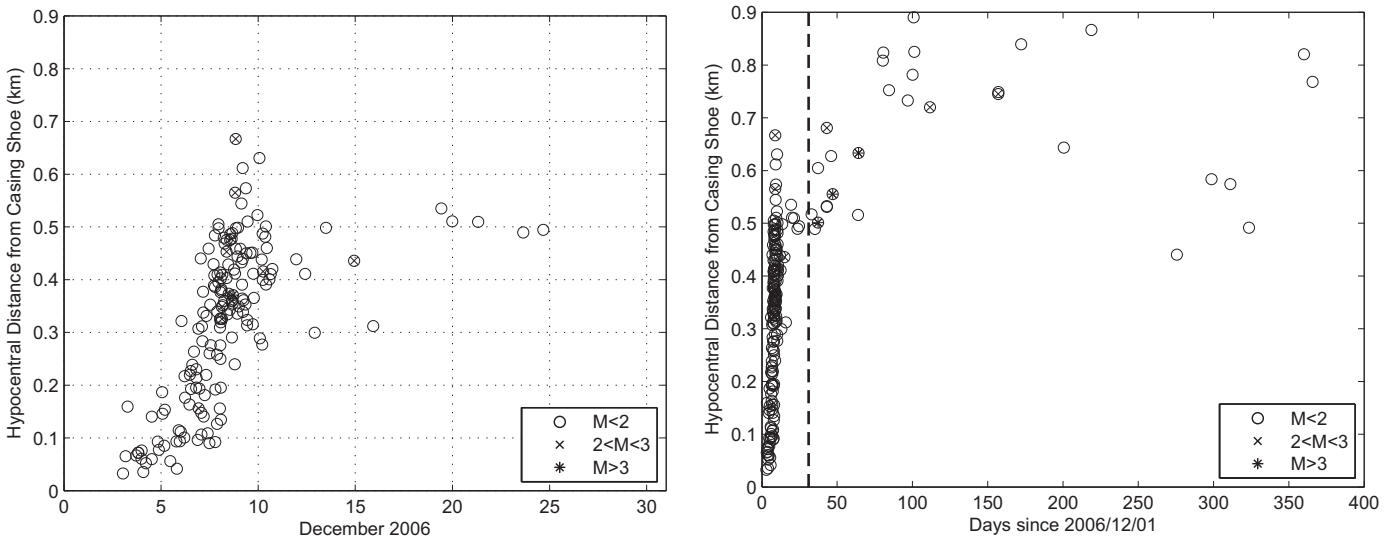

▲ **Figure 6.** Hypocentral distance of each event from the casing shoe determined from the master-event locations as a function of time. The left panel shows an enlargement of the first month included in the right panel, and the dashed vertical line on the right marks December 31, 2006.

all 195 events is 0.01 ± 0.006 s suggests that the assumed timing uncertainties, and thus also the computed standard location errors, are on the conservative side. It should be noted that this error analysis does not include possible errors due to wrong assumptions about the seismic velocities and their fluctuations in the hypocentral volume. However, a variation of ±0.1 km/s in *Vp* and assuming a constant *Vp/Vs* ratio causes an average change in the relative hypocenter parameters of less than 5 m. Since the source volume is located entirely in the crystalline basement at a depth between 4 and 5 km, where mean seismic velocities are not expected to vary by much, this source of error does not add significantly to the conservative uncertainty estimates of the relative locations.

However, the analysis of the relative location accuracy does not tell us anything about the absolute location accuracy of the hypocenters as a whole. Fortunately, during cementation of the casing inside the well, a sequence of seismic events was induced by the injection of the cement into the space between the casing and borehole wall. One of these events (2006/11/10 17:21 UTC) was strong enough to have been recorded by the SED network ($M_L = 0.7$). Given that the duration of this operation was only a matter of a few hours, and that consequently the injected fluid did not have enough time to migrate far from the well, it is reasonable to assume that the hypocenter of this event must be located only a few tens of meters from the borehole. The location relative to the chosen master event, calculated by the same procedure as described above, places it 37 m west and 2 m south of the borehole and 92 m above the casing shoe. Because the instrument in the deepest monitoring borehole (OTER2) was not operational at that time, the calculated standard deviation for this location is on the order of 60 m horizontally and 90 m vertically. Thus within the attainable precision, the adopted location procedure puts the epicenter of this cementation event in the immediate vicinity of the borehole, as expected. Conversely, it follows that the accuracy of the horizontal location of the master event is also around 50 m. Combining the estimated location uncertainty of the master event and the calculated average standard deviation of the relative locations, we conclude that the absolute epicenter location accuracy for all events is on the order of 100 m. These considerations, however, do not permit us to draw any conclusions about the accuracy of the absolute focal depths, because we don't know the exact depth at which the event that was induced by the cementation operations actually occurred. On the other hand, the *S* phase in the seismograms of the master event, which were recorded by the temporary seismometer in the injection borehole, cannot be clearly identified, so that the *S-P* time is certainly not more than about 0.01 s. Consequently, given that the calculated depth of the master event is practically the same as the depth of the temporary sensor, its vertical location error is at most on the order of ±80 m.

The following features of the resulting locations are worth noting:

- The overall hypocenter distribution defines a near-vertical plane that strikes NNW-SSE (Figure 5).
- A plot of radial distance of each event from the casing shoe as a function of time (Figure 6) shows an overall temporal migration away from the injection borehole, supporting the idea that the observed seismicity is induced by the diffusion of water away from the borehole.
- Of the post-stimulation events (defined here as those events that occurred after 10 December 2006, marked by the abrupt decrease in slope of the curve of the cumulative number of events in Figure 5), 80% are located at the periphery of the epicenter cloud, at distances between 500 and 900 m from the casing shoe (Figure 6).
- The events that occurred between 1 January and 2 February 2007 constitute a well-defined cluster of hypocenters in the upper SSE sector of the cloud (Figure 5).
- This cluster comprises the three $M_L > 3$ post-stimulation events recorded to date.

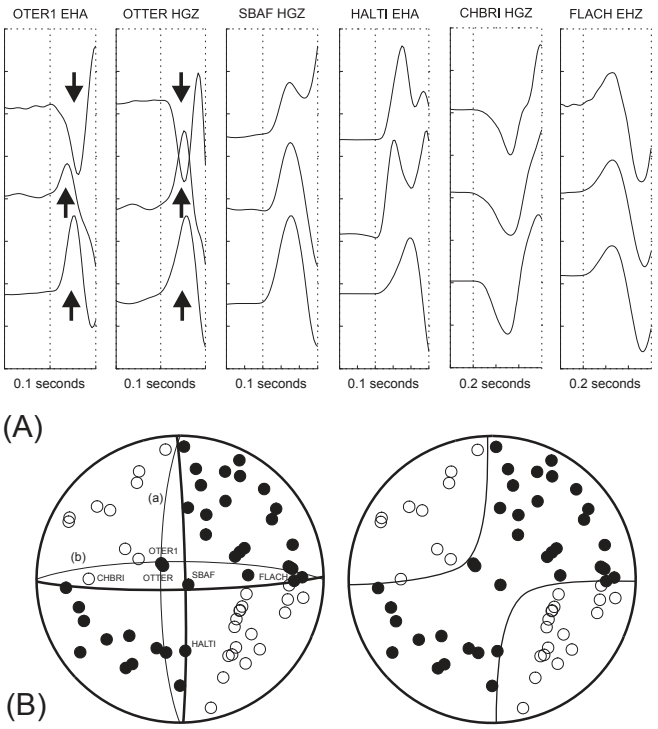

▲ **Figure 7.** (A) *P*-wave first motions of the $M_L > 3$ event from 2007 (event nos. 168, 174, and 176 in Figure 10) at the six stations labeled in the fault-plane solution below. The seismograms are all proportional to ground velocity and are filtered with a causal 2nd-order bandpass-filter between 1 and 20 Hz. Note the polarity reversal (arrows) at stations OTER1 and OTTER of the first event compared to the other two. (B) Fault-plane solution of the M_L 3.2 event of 2007/02/02 03:54 (event no. 176). The stereographs are lower hemisphere, equal area projections; solid circles correspond to compressive (upward) and empty circles to dilatational first motion (downward). Left: Double-couple solution with the preferred nodal planes (thick lines) and two alternatives (thin lines a and b). Right: Sketch of a possible non-double-couple solution with volume change (after Julian *et al.* 1998). See text for further explanations.

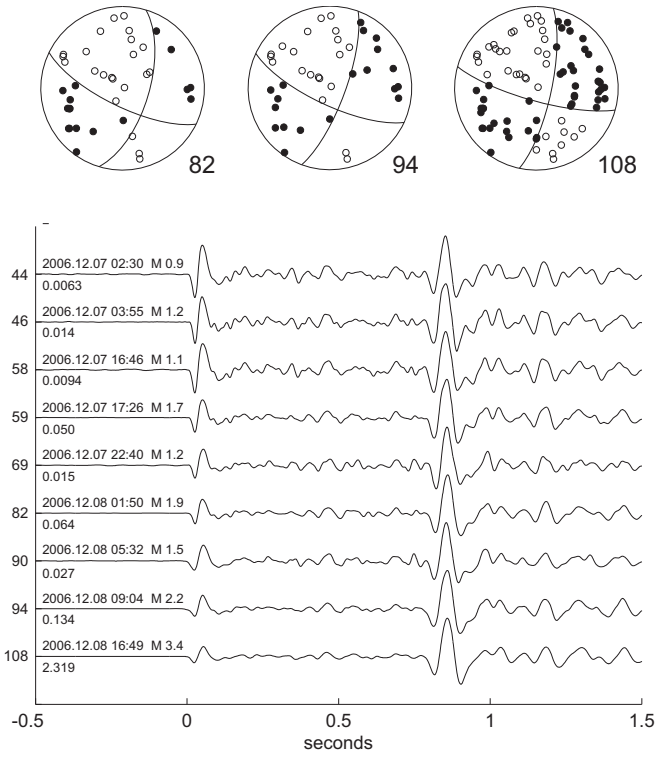

▲ **Figure 8.** Top: Fault-plane solutions of the M_L 3.4 mainshock and of two foreshocks that belong to the same cluster. The stereographs are lower hemisphere, equal area projections; solid circles correspond to compressive (upward) and empty circles to dilatational (downward) first motion. The number next to each stereograph corresponds to the event number in Figures 9 and 10. Bottom: Seismograms of the M_L 3.4 mainshock family recorded on the EHA component of the borehole sensor at OTER1, interpolated to 960 Hz and filtered with a causal 2nd-order 20-Hz low-pass filter. The event numbers are given to the left of the vertical axis and the number below the date, time, and M_L of each event denotes peak ground velocity of each trace (mm/s).

- Most of the recorded events that occurred after February 2 are also located in the upper SSE corner of the cloud.
- Notable exceptions to the previous point are the two outlier events to the south and east of the main cloud (Nos. 183 and 188 in Figure 6), which occurred on 11 March 11 (M_L 1.1) and 18 June 2007 (M_L 1.8); the seismograms and locations of these two events have been reviewed several times, and no reason was found to question the results; in fact, the latter event is part of a distinct cluster of smaller events recorded by GEL, which is offset from the main hypocenter cloud (U. Schanz, Geothermal Explorers Ltd., personal communication).

Given two independent sets of hypocenter locations (routine and master event), the obvious question to ask is how much they differ from each other. On average, the routine locations are shifted by 220 m to the south and 640 m to the east and are 460 m deeper with respect to the master-event relocations. As discussed above, the computed uncertainties of the relative locations are on the order of 50 m horizontally and 70 m vertically, and the absolute error of the location of the master event itself is certainly less than 100 m. Thus the bias of, on average, 0.7 km to the ESE of the routine locations is real and is probably due to the fact that the 3D regional velocity model does not have sufficient resolution to account correctly for the local near-surface velocity structure below Basel. Note, however, that both the horizontal and vertical errors are within the uncertainties of 1 to 1.2 km computed by the routine location algorithm.

Moreover, the scatter (in terms of computed standard deviations) of the differences between routine and master-event locations is 85 m in the N-S direction, 166 m in the E-W direction, and 377 m in depth. For the horizontal coordinates these values correspond to about one to two times the rounding errors of the routine locations, so that on average the routine locations give a faithful picture of the epicenter distribution.

However, in depth the scatter is four times the rounding errors of the output, so that the focal depths calculated routinely by SED are not sufficiently reliable for any significant conclusions in the context of the reservoir stimulation.

FOCAL MECHANISMS

Focal mechanisms based on first-motion polarities were determined for the 28 strongest events that occurred between 3 December 2006 and 6 May 2007. In a first stage, locations, azimuth, and vertical take-off angles were calculated with the routine location procedure and the regional 3D velocity model. Subsequently it became clear that the average bias of 700 m to the ESE of the routine locations relative to the master-event locations causes significant errors in azimuth and take-off angles calculated for the near-epicenter stations. Thus, epicentral distances and azimuths for all stations located at distances less than 16 km were corrected on the basis of the master-event locations. As explained in more detail by Deichmann and Ernst (forthcoming), the vertical take-off angles were calculated with a 2D ray-tracing program (Gebrande 1976), taking into account the lateral variations of the near-surface structure.

The stereographs corresponding to parameters of all 28 events are reproduced in Deichmann and Ernst (forthcoming), and the corresponding parameters are listed in Table 3. The stereographic plots with the individual first motions of the M_L 3.4 mainshock and of two of its foreshocks that belong to the same subcluster are also shown in Figure 8. Given the large number of temporary stations installed in the epicentral area, the focal sphere is well sampled even for events as small as M_L 1.7, and the resulting mechanisms are well constrained. Nevertheless, in some cases discrepant first-motion polarities could not be avoided. In fitting the observed polarities we always attempted to define the nodal planes in such a way as to maximize the number of matching polarities. As a result, most of the discrepancies are observed at stations OTTER, OTER1, and

TABLE 3
Focal mechanism parameters of the induced seismicity based on first-motion polarities. Evn: event number; Time: UTC; Z: focal depth (km); M: local magnitude (ML) calculated by SED; Nodal Planes: strike/dip/rake; P- and T- Axes: azimuth/plunge. The events are numbered sequentially as recorded by SED, starting with the ML 0.8 event of Dec. 3rd, 00:59, UTC.

Evn	Date	Time	Lat	Lon	Z	M	Plane 1	Plane 2	P	T
005	2006/12/03	19:51	47.586	7.594	4.4	1.7	176/64/ 004	084/86/ 154	133/15	037/21
039	2006/12/06	22:27	47.587	7.593	4.2	2.2	154/42/-062	298/54/-113	152/71	044/06
043	2006/12/07	01:44	47.586	7.592	4.4	1.9	310/47/-123	173/52/-060	146/67	242/03
081	2006/12/08	01:49	47.587	7.592	4.5	1.9	096/80/-178	006/88/-010	320/08	051/06
082	2006/12/08	01:50	47.584	7.594	4.7	1.9	017/63/-020	116/72/-152	338/32	245/06
086	2006/12/08	03:06	47.585	7.595	4.1	2.6	089/78/-178	359/88/-012	313/10	044/07
087	2006/12/08	03:24	47.583	7.594	4.8	2.3	072/80/ 172	163/82/ 010	298/01	028/13
093	2006/12/08	09:02	47.583	7.596	4.2	1.8	178/65/ 007	085/84/ 155	134/13	039/22
094	2006/12/08	09:04	47.585	7.593	4.8	2.2	115/73/-164	020/75/-018	337/23	068/01
098	2006/12/08	11:36	47.584	7.596	4.6	2.2	114/82/ 180	204/90/ 008	339/06	069/06
102	2006/12/08	15:13	47.583	7.595	4.7	2	078/52/-160	335/74/-040	290/39	031/14
103	2006/12/08	15:30	47.585	7.594	4.1	1.8	190/58/ 009	095/82/ 148	146/16	048/28
104	2006/12/08	15:31	47.585	7.595	4	2.1	179/62/ 007	086/84/ 152	136/15	039/24
105	2006/12/08	15:47	47.588	7.593	4.1	2.7	097/80/-177	006/87/-010	321/09	052/05
108	2006/12/08	16:49	47.584	7.593	4.7	3.4	012/75/-013	105/77/-165	329/20	238/02
112	2006/12/08	19:27	47.582	7.596	4.7	2.3	077/58/-177	345/87/-032	296/24	036/20
113	2006/12/08	20:20	47.583	7.594	5	2.5	008/53/-028	115/68/-140	337/43	238/09
147	2006/12/10	06:11	47.584	7.595	4	2	182/75/ 012	089/78/ 165	136/02	045/19
159	2006/12/14	22:39	47.584	7.595	4	2.5	186/61/ 018	087/74/ 150	139/08	043/32
162	2006/12/19	23:50	47.584	7.595	3.9	1.8	185/61/ 018	086/74/ 150	138/08	042/32
167	2007/01/04	04:38	47.583	7.596	4.1	1.8	174/65/ 006	082/85/ 155	131/14	035/21
168	2007/01/06	07:20	47.582	7.596	4.2	3.1	091/79/-176	360/86/-011	315/11	046/05
170	2007/01/12	03:35	47.581	7.597	4.2	2.2	082/79/ 180	172/90/ 011	306/08	038/08
173	2007/01/15	00:03	47.582	7.596	4	1.9	182/73/ 006	090/84/ 163	137/08	045/16
174	2007/01/16	00:09	47.582	7.596	4.1	3.2	091/83/-176	001/86/-007	316/08	046/02
176	2007/02/02	03:54	47.582	7.596	4	3.2	089/84/-177	359/87/-006	314/06	044/02
184	2007/03/21	16:45	47.581	7.596	4	2.8	085/75/-175	354/85/-015	308/14	040/07
185	2007/05/06	00:34	47.581	7.596	4	2.3	080/80/ 171	172/81/ 010	306/01	036/13

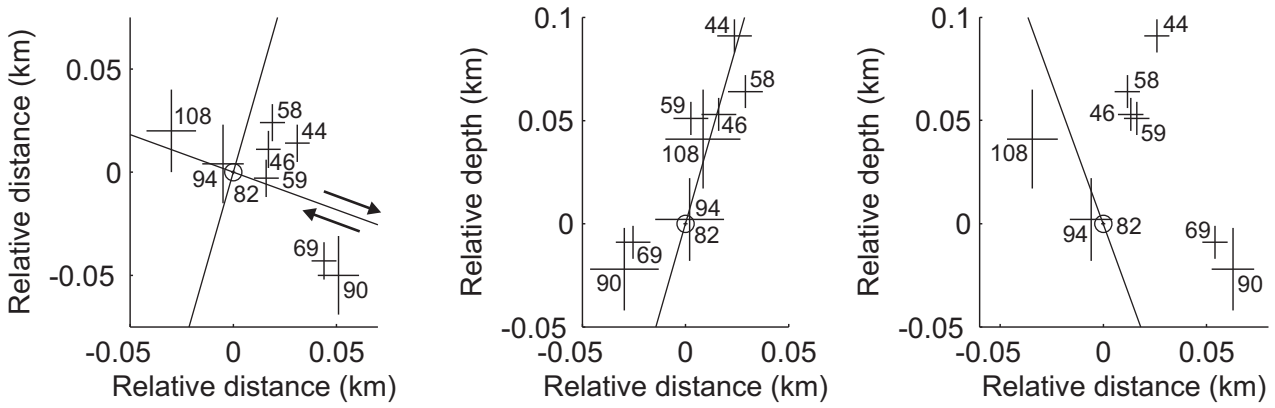

▲ **Figure 9.** Result of the correlation-based relative locations of the mainshock family. Left panel: Epicenters with traces of the two nodal planes of the average focal mechanism for events 82, 94, and 108; the arrows identify the sense of slip on the active fault plane. Center panel: Depth cross-section with the trace of the active WNW-ESE striking fault plane. Right panel: Depth cross-section with the trace of the NNE-SSW striking nodal plane. The master event is number 82 and the M_L 3.4 event is number 108. The size of each cross corresponds to the location uncertainty (one standard deviation).

OTER2. Given the small location uncertainty of these events, it is highly unlikely that the inconsistent polarities are due to location errors, despite the fact that these stations are located at short epicentral distances. As an illustration of the inconsistent polarities, Figure 7 shows selected first motions for the three $M_L > 3$ events of 2007 and an enlargement of the fault-plane solution of the event of 2007/02/02 (no. 176). The polarities of the first of these events (2007/01/06, no. 168) are fully compatible with a well-constrained pure double-couple solution. The first motions at stations OTER1 and OTTER are downward for this event, whereas for the other two events the first motions at these two stations are upward (Figure 7). If one were to seek a solution that satisfies these two upward polarities for the latter two events, one could not avoid discrepancies at other stations such as SBAF, HALTI, CHBRI, and FLACH (Figure 7B, left-hand diagram),which have the same first-motion directions for all three events. Taken by themselves, and given that stations OTER1 and OTTER as well as SBAF and HALTI are located at small epicentral distances, it could be argued that the discrepant first motions for the two events of 2007/01/16 and 2007/02/02 (nos. 174 and 176) are due to hypocenter mislocations or wrong take-off angles. However, all three $M_L > 3$ events of 2007 are part of the same event cluster that occupies a source region no larger than 300 x 300 m (see Figure 5). Given the close relative proximity of the hypocenters of these three events, discordant polarities would have to be observed for all three events, if they were due to location errors or to unmodeled path effects. Therefore, the discordant polarities observed for two of these events must be a source effect and are an indication of non-double-couple components of the focal mechanism that cannot be accounted for by a standard double-couple fault-plane solution. A possible alternative solution is sketched in the right-hand diagram of Figure 7(B), which corresponds to a combination of a double-couple and an isotropic moment tensor component with a net positive volume change (after Julian *et al.* 1998, Figure 11). The same could also apply to the discordant first motions observed for the events of 8 December 2006, 03:06, and 6 May 2007 (Deichmann and Ernst forthcoming). The possibility of a significant non-double-couple component in these focal mechanisms raises the question of whether other events might also have focal mechanisms with non-double-couple components that are not visible in the fault-plane solution as discordant polarities because of the fewer number of observations compared to these stronger events. A more rigorous test of this hypothesis, based not only on the first-motion polarities but also an analysis of the observed amplitudes, is the subject of a separate study that is underway.

THE MAINSHOCK FAULT PLANE

Of the two nodal planes, the one that corresponds to the fault plane on which the earthquake rupture actually took place cannot be identified based on the focal mechanism alone. Both for the derivation of the local stress field and for characterizing the permeability enhancement induced by the water injection, knowledge of the active fault planes would be particularly useful. The standard method for obtaining this information consists of identifying families of earthquakes with similar waveforms and determining precise relative locations of the hypocenters of the individual events in these families (*e.g.*, Deichmann and Garcia-Fernandez 1992). The waveform similarity ensures that the focal mechanisms of these events are the same, and experience shows that their hypocenters lie on a plane that matches one of the nodal planes and that thus defines the active fault. The principles for determining sufficiently precise locations are the same as discussed in the context of the master-event locations, except that the similarity of the waveforms of the different events recorded at a given station lets us use a cross-correlation technique to reduce the uncertainty of the relative arrival times to a few milliseconds.

Such an approach has already been applied to the Basel data by Kumano *et al.* (2007) and Häring *et al.* (2008). The latter identify the more or less N-S striking nodal plane as the active one for events nos. 5 and 112 as well as for the pair 173 and 176

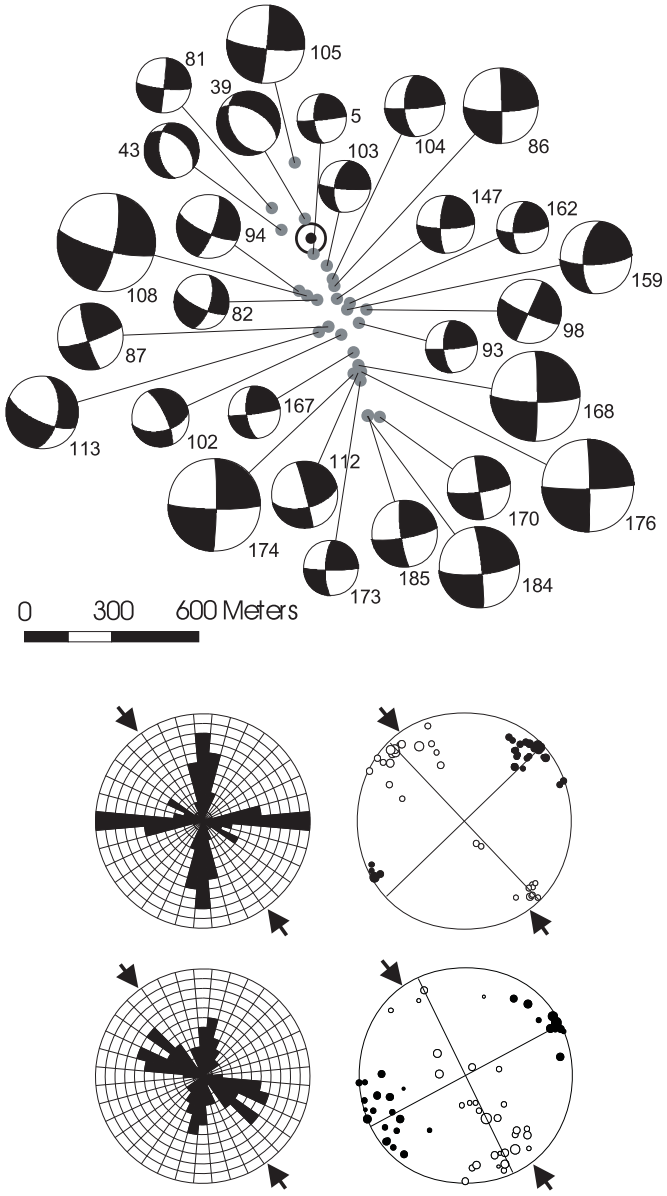

▲ **Figure 10.** Top: Epicenter map with master-event locations and focal mechanisms. The size of each stereograph is proportional to magnitude ($1.7 \le M_L \le 3.4$) and the numbers correspond to the event numbers in Table 3. The location of the Basel geothermal well is indicated by the circle with the black dot. Note that even at this scale the three events 82, 94, and 108, which are part of the mainshock family and have almost identical focal mechanisms, stand out as a distinct cluster. Bottom: Symmetric polar histograms (rose diagrams) of the strike of the focal mechanism nodal planes and stereographic equal area plots of the *P*-axes (empty circles) and the *T*-axes (black circles) for the 28 induced events (top) and for the 30 naturally occurring earthquakes (bottom). The arrows point in the direction of the maximum horizontal compressive stress derived from wellbore failure measurements in the crystalline basement down to 5 km depth by Valley and Evans (2006, forthcoming).

(see Figure 10 and Table 3), whereas for event no. 93 the active plane strikes E-W. Noting the striking similarity of the focal mechanisms of the M_L 3.4 mainshock (no. 108) and of events nos. 82 and 94 shown in Figure 8, and given their similar hypocenter locations, we searched the available data for additional closely located events with similar waveforms. We found a total of nine such events. As can be seen in Figure 8, the seismograms recorded at the borehole station OTER1 are similar enough for cross-correlations, but the *P*- to *S*-wave amplitude ratios are not identical. In fact, we also observe a polarity change at station JOHAN, where the first onset is upward for the first six events and downward or nodal for the other three events. Consequently, the focal mechanisms of these events are not entirely identical, a fact that is also reflected in a difference of up to 10 degrees in the strike of the nodal planes between the three events of this cluster for which focal mechanisms are available (events 82, 94, and 108 in Figure 10). However, as corroborated by the results presented below, these small differences do not contradict the hypothesis of a common fault for these events but are probably just evidence of a non-planar fault and possible differences in rake. Nevertheless, in order to maximize the number of available records with sufficient similarity for the cross-correlation, we subdivided the family of nine events into two subsets, with event no. 82, which has a high similarity with all events, as the master event for both subsets. We used the *P* phase at JOHAN and MATTE only for the correlation of the first subset. The other phases used are JOHAN (*S*), MATTE (*S*), OTER1 (*P* and *S*), RIEH2 (*P* and *S*), HALTI (*P* and *S*), and OTER2 (*S*). Given the large magnitude range between the smallest and largest event over the whole family, the signal similarity was optimized by applying a causal 2nd order, 20-Hz low-pass filter to the data. In addition, before the correlation, the traces were interpolated by adding the appropriate number of zeros to the Fourier spectrum to increase the sampling rate to 960 Hz in the case of OTER1 and to 1,000 Hz for all other stations. To assess the quality of the cross-correlations, we performed the operation with all possible combinations of master events in each subfamily and then derived the optimal arrival times relative to the initially chosen master event through a least-squares adjustment of the discrepancies between the various combinations (see the Appendix in Deichmann and Garcia-Fernandez 1992 for details of the procedure). The remaining relative arrival-time uncertainties range between 1.2 and 5.7 ms, depending on the number of traces and the number of master-event combinations used for the cross-correlation. Given that the relative hypocentral distances within a particular family are small compared to the distance to the nearest stations, we could apply a linear location algorithm, for which the azimuth and take-off angle are assumed to be constant (Console and DiGiovambattista 1987). The results shown in Figure 9 demonstrate that the relative hypocenters of these nine events form a cluster that coincides much better with the WNW-ESE than with the NNE-SSW striking nodal plane. Moreover, the rms of the travel-time residuals that result from the relative location procedure range between 0.8 and 2.5 ms, which confirms that the uncertainty estimates defined by the size of the crosses in Figure 9 are realistic.

Thus the conclusion from this exercise is that the M_L 3.4 mainshock and the preceding eight events belonging to the same family were caused by dextral strike-slip motion on a steeply dipping WNW-ESE striking fault. The hypocenters of the available events cover a fault patch with a diameter of about 150 m. However, this dimension is a lower bound, because it does not include the rupture dimension of the individual events. In fact, the mainshock itself, which is located at the edge of this cluster, is likely to extend the active fault patch by roughly another 100 m in a WNW direction.

DISCUSSION

Figure 10 shows the resulting focal mechanisms (or at least their double-couple components) on an epicenter map with the master-event relocations. A polar histogram with the strike of all nodal planes and a stereographic plot with the orientation of all *P*- and *T*-axes is shown in Figure 10 as well. According to the criteria of the World Stress Map Project (Zoback 1992), of the 28 fault-plane solutions two are normal faulting mechanisms and one is a strike-slip mechanism with a strong normal component. All others are typical strike-slip mechanisms with mostly NS and EW striking nodal planes. As a consequence, the *T*-axes are all nearly horizontal and oriented in a NE or SW direction (mean azimuth 46 ± 11 degrees) and the *P*-axes of the strike-slip events point in a NW or SE direction (mean azimuth 138 ± 13 degrees). Given the relatively small scatter of the orientations of the *P*- and *T*-axes and knowledge of the active fault plane for only a few events, a formal stress inversion would not be particularly well constrained.

Nevertheless it is instructive to compare the *P*- and *T*-axes of the induced seismicity with those of the naturally occurring earthquakes in the region of Basel (Figure 10). As documented in earlier studies, the focal mechanisms available until 1999 for the southern Rhine Graben, the Black Forest, and northern Switzerland south of Basel are dominated by strike-slip and normal faulting mechanisms (Plenefisch and Bonjer 1997; Evans and Roth 1998; Kastrup *et al.* 2004). A few more-recent events documented in the annual reports of the Swiss Seismological Service are of the same type. Therefore the most stable measure of the horizontal component of the predominant deformation is the azimuth of the *T*-axes. For a comparison between the natural and the induced seismicity, we selected the 30 available focal mechanisms in a 30 x 30-km large region south of latitude 47.66 and east of longitude 7.5 (Figure 1 and Table 1).

This selection includes a representative number of events from both the Rhine Graben and the Jura south of Basel but excludes the relatively large number of focal mechanisms of the Sierentz cluster in the north, which would otherwise tend to dominate the picture (Bonjer 1997). The average azimuth of the *T*-axes of these 30 focal mechanisms is 62 ± 15 degrees. This value is both stable and representative of the region around Basel: the corresponding value for the 18 strike-slip events alone is 65 ± 14 degrees, for the 16 events shallower than 15 km it is 59±13 degrees, and for the 21 events in a smaller zone closer to Basel it is 63 ± 16 degrees. The corresponding median values deviate from these means by only one or two degrees. The mean azimuth of 46 ± 11 degrees derived for the induced seismicity differs by roughly 15 to 20 degrees from these values. However, considering the large overlap of the scatter of these values and the small crustal volume that is sampled by the induced earthquakes as well as the fact that the focal depths of the majority of natural events for which focal mechanisms are available are considerably deeper, this difference cannot be considered significant evidence for an anomalous behavior caused by the water injection. This conclusion is also supported by noting that the average value for the direction of the regional least compressive horizontal stress, S_h, calculated by Kastrup *et al.* (2004) by two different inversion methods from the focal mechanisms in the southern Rhine Graben region and in the central part of northern Switzerland, is about 54 degrees and is thus just as compatible with the induced seismicity as with the natural seismicity from which it was derived. Moreover, this value is identical to the average local orientation of S_h in the crystalline basement derived from wellbore failure measurements in the 5-km-deep Basel borehole by Valley and Evans (2006, forthcoming).

A comparison of the azimuthal histograms of the nodal-plane orientations, shown in Figure 10, indicates that the more or less N-S striking nodal planes of the induced seismicity are also well represented in the natural seismicity. However, the E-W striking nodal planes that stand out in the distribution of the induced events (see Figure 10) are largely missing in the histogram of the natural seismicity. Given the mean orientation of S_H of 144 ± 14° calculated by Valley and Evans (2006, forthcoming) from borehole breakouts and drilling-induced tensile fractures observed in the borehole, we would expect the N-S striking nodal planes to be more favorably oriented relative to the ambient stress field than the E-W striking planes. From a first analysis presented by Häring *et al.* (2008) of a few clusters of similar events, analogous to the analysis performed in this study for the M_L 3.4 mainshock, it seems that the stimulation has activated strike-slip shear dislocation on both the N-S and the E-W striking fault planes. Given that the microseismic cloud as a whole is oriented in a NNW-SSE direction (approximately 156 degrees E from N) and that only two of the 56 nodal planes of the induced events available to date strike more or less in this direction, it is reasonable to assume that the injected water, as it migrates away from the borehole, will create a flow path that links up a sequence of fractures oriented in an E-W as well as in a N-S direction (Häring *et al.* 2008). It is also possible that some of the faults activated by the increased water pressure constitute branches that do not link up with other faults but finish in a dead end and thus do not contribute to an overall permeability enhancement. Note that the mainshock cluster, which occurred on a WNW-ESE striking fault, deviates from this prominent N-S and E-W pattern of nodal planes, but it coincides with one of the maxima in the nodal-plane histogram of the natural seismicity (Figure 10).

Based on the observation that the overall strike of the microseismic cloud is closer to a N-S than to an E-W orientation and that slip on the N-S striking faults is favored by the ambient stress field, we would expect a larger proportion of the total seis-

mic moment to have been released on these N-S striking faults. The N-S oriented nodal planes agree also with the strike of the active fault plane identified in the Pratteln sequence, located 10 km southeast of the Basel geothermal site (Faber *et al.* 1994), as well as with the orientation of the eastern border fault of the Rhine Graben and with the strike of the Reinach fault, which is considered to be a possible host of the 1356 Basel earthquake (Meghraoui *et al.* 2001). Slip on the less favorably oriented E-W striking faults would thus have been enabled by the effect of the increased pore pressure. It is also noteworthy that the NW-SE striking fractures observed in the borehole logs, as reported by Häring *et al.* (2008), are practically missing in the fault-plane population of both the natural and the induced seismicity. Given that these fractures are perpendicular to the breakouts observed in the same borehole, they are more likely drilling induced tensile fractures, as interpreted by Valley and Evans (2006, forthcoming), than traces of naturally occurring faults.

In summary, despite the evidence for possible non-double-couple components for some of the focal mechanisms, the available fault-plane solutions support the view that the seismicity induced by the water injection below Basel occurred predominantly as shear dislocation on pre-existing faults. The temporal and spatial evolution of the observed seismicity is clearly a consequence of the increased pore pressure due to the injected water. However, according to Häring *et al.* (2008), the water pressure in the formation did not reach the least compressive stress necessary for hydrofracking, and, as documented in this article, most of the seismic activity occurred long before and long after the well-head pressure reached its maximum level. Therefore the injected water, by decreasing the effective stress on pre-existing fractures, acted only as a trigger, while the driving agent was the ambient tectonic stress.

CONCLUSIONS

The 195 seismic events recorded by the network of the Swiss Seismological Service and analyzed in this article constitute only a tiny fraction of the total number of events induced since 2 December 2006 by the geothermal reservoir stimulation in Basel. However, because these are the strongest events, it is crucial that we analyze and understand the seismotectonic context in which they occurred. The conclusions of this study can be summarized as follows:

- The structure and orientation of the stimulated rock volume is well resolved even by this relatively small subset of events; a prerequisite for obtaining the necessary resolution of the hypocenter locations is the accurate knowledge of the location of a suitable reference event; this can be obtained with a check-shot in the injection well or, as was done in the present case, by operating a borehole sensor in the injection well during the first stages of the stimulation (Häring *et al.* 2008).
- With continuing injection, the seismicity migrates away from the borehole, as would be expected from a diffusion process; after shut-in and bleed-off, seismic activity is concentrated at the periphery of the stimulated volume.
- Three of the four strongest events occurred one to two months after stimulation had been stopped and after the water pressure in the borehole had returned to hydrostatic levels.
- Although some of the focal mechanisms show signs of non-double-couple components with a volume change, overall the results are compatible with shear failure on pre-existing faults. Contrary to intuition, the most convincing evidence for signs of volume change are not found in the events that occurred at the peak of the stimulation when the pressure was highest, but in some of the events that occurred long after stimulation had been stopped and water pressure had presumably dropped again.
- From the high-precision hypocenter locations of the earthquake family that includes the M_L 3.4 mainshock, we conclude that this event occurred as dextral strike-slip motion on a steeply dipping WNW-ESE striking fault. Moreover, with a strike of 30–40 degrees relative to the direction of S_H, this fault is oriented favorably with respect to the ambient stress field.
- Most of the induced seismicity occurred before and after water pressure in the formation came even close to the least compressive stress. In addition, the observed focal mechanisms are in good accord with what would be expected from both the in-situ stress observations and the stress field derived from the previously known natural seismicity. Both of these observations support the conclusion that the earthquakes induced by the reservoir stimulation below Basel, rather than representing a case of hydrofracking, occurred mainly as shear dislocation on pre-existing faults triggered by the increase in pore pressure due to the injected water but driven by the ambient tectonic stress.

Ongoing research will attempt to analyze in more detail the relationship between the focal mechanisms and hypocenter alignments and to clarify the nature of possible non-double-couple mechanisms. A key to assessing the permeability enhancement associated with the seismicity induced during the reservoir stimulation below Basel will also be a quantification of the source dimensions and dislocations associated with the observed seismic events as a function of space and time.

ACKNOWLEDGMENTS

This study would not have been possible without the cooperation of Geothermal Explorers Ltd., who gave us real-time access to the data of their borehole sensors, and part of this work was done with financial support by Geopower Basel AG; both contributions are gratefully acknowledged. Moreover, part of this work constitutes a contribution to the interdisciplinary research project GEOTHERM, funded by the Competence Center of Environment and Sustainability (CCES) of ETH (http://www.cces.ethz.ch/projects/nature/geotherm/). We also thank W. Brüstle and S. Stange of the Landeserdbebendienst Baden-Württemberg in Freiburg for sending us all their waveform data, which were crucial for much of this study. Thanks are also due to C. Bachmann and S. Wöhlbier, who contributed

to this article with a statistical analysis of the magnitudes and helped with several of the figures, as well as to C. Bärlocher and his colleagues at the electronics lab of SED and to M. Baer for their efforts in establishing and maintaining access to the data of the borehole stations in Basel. Keith Evans and an anonymous reviewer carefully reviewed the original manuscript and made several helpful suggestions for improvements. We thank Stefan Baisch for pointing out a significant mistake in an earlier version of the conclusions.

REFERENCES

Asanuma, H., Y. Kumano, A. Hotta, U. Schanz, H. Niitsuma, and M. Häring (2007). Analysis of microseismic events from a stimulation at Basel, Switzerland. *GRC Transactions* **31**, 265–269.

Baer, M., N. Deichmann, J. Braunmiller, D. Ballarin Dolfin, F. Bay, F. Bernardi, B. Delouis, *et al.* (2001). Earthquakes in Switzerland and surrounding regions during 2000. *Eclogae Geologicae Helvetiae* **94** (2), 253–264.

Baer, M., N. Deichmann, J. Braunmiller, S. Husen, D. Fäh, D. Giardini, P. Kästli, U. Kradolfer, and S. Wiemer (2005). Earthquakes in Switzerland and surrounding regions during 2004. *Eclogae Geologicae Helvetiae/Swiss Journal of Geosciences* **98** (3), 407–418; doi: 10.1007/s00015-005-1168-3.

Bonjer, K.-P. (1997). Seismicity pattern and style of seismic faulting at the eastern borderfault of the southern Rhine Graben. *Tectonophysics* **275**, 41–69.

Console, R., and R. DiGiovambattista (1987). Local earthquake relative location by digital records. *Physics of the Earth and Planetary Interiors* **47**, 43–49.

Deichmann, N. (1987). Seismizität der Nordschweiz, 1983–1986. Nagra Technischer Bericht, NTB 87-05, Swiss National Cooperative for Radioactive Disposal (NAGRA).

Deichmann, N., and J. Ernst (forthcoming). Earthquake focal mechanisms of the induced seismicity in 2006 and 2007 below Basel (Switzerland). *Swiss Journal of Geosciences* **102** (3).

Deichmann, N., and M. Garcia-Fernandez (1992). Rupture geometry from high-precision relative hypocenter locations of microearthquake clusters. *Geophysical Journal International* **110**, 501–517.

Deichmann, N., M. Baer, J. Braunmiller, D. Ballarin Dolfin, F. Bay, F. Bernardi, B. Delouis, *et al.* (2002). Earthquakes in Switzerland and surrounding regions during 2001. *Eclogae Geologicae Helvetiae/Swiss Journal of Geosciences* **95** (2), 249–261.

Deichmann, N., M. Baer, J. Braunmiller, C. Cornou, D. Fäh, D. Giardini, M. Gisler, *et al.* (2004). Earthquakes in Switzerland and surrounding regions during 2003. *Eclogae Geologicae Helvetiae/Swiss Journal of Geosciences* **97** (3), 447–458.

Deichmann, N., D. Ballarin Dolfin, and U. Kastrup (2000). Seismizität der Nord- und Zentralschweiz. Nagra Technischer Bericht, NTB 00-05, Nagra, Wettingen.

Dyer, B. C., U. Schanz, F. Ladner, M. O. Häring, and T. Spillmann (2008). Microseismic imaging of a geothermal reservoir stimulation. *The Leading Edge* **27**, 856–869.

Evans, K. F., and P. Roth (1998). *The State of Stress in Northern Switzerland Inferred from Earthquake Seismological Data and In-situ Stress Measurements*. Report prepared for the Deep Heat Mining (DHM) Project Basel on behalf of Geothermal Explorers Ltd., Pratteln, Switzerland, 26 pps.

Faber, S., K.-P. Bonjer, W. Brüstle, and N. Deichmann (1994). Seismicity and structural complexity of the Dinkelberg block, southern Rhine Graben. *Geophysical Journal International* **116**, 393–408.

Gebrande, H. (1976). A seismic ray-tracing method for two-dimensional inhomogeneous media. In *Explosion Seismology in Central Europe*, ed. P. Giese, C. Prodehl, and A. Stein, 162–167. Berlin: Springer.

Häring, M. O., U. Schanz, F. Ladner, and B. C. Dyer (2008). Characterization of the Basel 1 enhanced geothermal system. *Geothermics* **37**, 469–495; doi:10.1016/j.geothermics.2008.06.002.

Husen, S., E. Kissling, N. Deichmann, S. Wiemer, D. Giardini, and M. Baer (2003). Probabilistic earthquake location in complex three-dimensional velocity models: Application to Switzerland. *Journal of Geophysical Research* **108** (B2), 2,077–2,096.

Julian, B. R., A. D. Miller, and G. R. Foulger (1998). Non-double-couple earthquakes, 1 Theory. *Reviews of Geophysics* **36** (4), 525–549.

Kastrup, U., M.-L. Zoback, N. Deichmann, K. Evans, D. Giardini, and A. J. Michael (2004). Stress field variations in the Swiss Alps and the northern Alpine foreland derived from inversion of fault plane solutions. *Journal of Geophysical Research* **109** (B1); doi:10.1029/2003JB002550B01402.

Kraft, T., P. M. Mai, S. Wiemer, N. Deichmann J. Ripperger, Ph. Kästli, C. Bachmann, D. Fäh, J. Wössner, and D. Giardini (2009). Mitigating Risk for Enhanced Geothermal Systems in Urban Areas. *EOS Trans. Am. Geophys. Union* **90** (32), 237–264.

Kumano, Y., H. Asanuma, A. Hotta, H. Niitsuma, U. Schanz, and M. Häring (2007). *Reservoir Structure Delineation by Microseismic Multiplet Analysis at Basel, Switzerland, 2006*. Paper presented at the 77th SEG meeting, San Antonio, TX, USA, Extended Abstracts, 1,271–1,276.

Meghraoui, M., B. Delouis, M. Ferry, D. Giardini, P. Huggenberger, I. Spottke, and M. Granet (2001). Active normal faulting in the Upper Rhine Graben and paleoseismic identification of the 1356 Basel earthquake. *Science* **293**, 2,070–2,073.

Plenefisch, T., and K.-P. Bonjer (1997). The stress field in the Rhine Graben area inferred from earthquake focal mechanisms and estimation of frictional parameters. *Tectonophysics* **275**, 71–97.

Ripperger, J., P. Kästli, and D. Fäh (forthcoming). Ground motion and macro-seismic intensities of a seismic event related to geothermal reservoir stimulation below the city of Basel—observations and modelling. *Geophysical Journal International*.

SED (2007). *Evaluation of the Induced Seismicity in Basel 2006/2007—Locations, Magnitudes, Focal Mechanisms, Statistical Forecasts and Earthquake Scenarios*. Report of the Swiss Seismological Service to Geopower Basel AG, December 2007.

Ustaszewski, K., and S. M. Schmid (2007). Latest Pliocene to recent thick-skinned tectonics at the Upper Rhine Graben–Jura Mountains junction. *Swiss Journal of Geosciences* **100**, 293–312.

Valley, B., and K. F. Evans (2006). *Stress Orientation at the Basel Geothermal Site from Wellbore Failure Analysis in BS1*. Report to Geopower Basel AG for Swiss Deep Heat Mining Project Basel. ETH Report No. ETH 3465/56. Ingenieurgeologie ETH Zürich, Switzerland, 29 pps.

Valley, B., and K. F. Evans (forthcoming). Stress orientation to 5 km depth in the basement below Basel (Switzerland) from borehole failure analysis. *Swiss Journal of Geosciences* **102** (3).

Zoback, M. L. (1992) First- and second-order patterns of stress in the lithosphere: The World Stress Map project. *Journal of Geophysical Research* **97** (B8), 11,703–11,711.

Swiss Seismological Service
ETH Zürich
Sonneggstrasse 5
CH-8092 Zürich, Switzerland
deichmann@sed.ethz.ch
(N. D.)